International Journal of Nanomedicine

Dovepress
Taylor & Francis Group

Open Access Full Text Article

ORIGINAL RESEARCH

Tumor Microenvironment Responsive and Platelet Membrane Coated Polydopamine Nanoparticles for Cancer Radiosensitization by Inducing Cuproptosis

Le Xin[1], Shipeng Ning[2], Hongwei Wang[1,3], Runze Shi[4]

[1]Department of General Surgery, Longgang Central Hospital of Shenzhen, Shenzhen, 518116, People's Republic of China; [2]Department of Breast Surgery, The Second Affiliated Hospital of Guangxi Medical University, Nanning, Guangxi, 530031, People's Republic of China; [3]Department of General Surgery, Guangdong Provincial Key Laboratory of Precision Medicine for Gastrointestinal Tumor, Nanfang Hospital, Southern Medical University, Guangzhou, Guangdong, 510515, People's Republic of China; [4]The Second Ward of Breast Surgery, Cancer Hospital Affiliated to Harbin Medical University, Harbin, 150086, People's Republic of China

Correspondence: Hongwei Wang; Runze Shi, Email 360873476@qq.com; shirz@hrbmu.edu.cn

Background: Cuproptosis, distinguished from apoptosis, necroptosis, pyroptosis, and ferroptosis, is a current form of programmed cell death that provides novel strategies for tumor therapy. Nanotechnology inducing cuproptosis showed potential in tumor ablation. However, these strategies might induce cellular damage due to a lack of tumor-targeting ability or insufficient tumor inhibition alone.
Methods: Here, biomimetic copper-doped polydopamine nanoparticles (PC NPs) were developed to specifically induce tumor cell cuproptosis to enhance radiotherapy (RT). PC NPs were characterized before application for tumor ablation.
Results: These PC NPs improve tumor targeting and accumulation. After entering the tumor region, PC degrades in cells responsive to acidic tumor microenvironment (TME). Next, Cu^{2+} is reduced to Cu^{+} after consuming overexpressed glutathione (GSH), which induces dihydrolipoamide S-acetyltransferase (DLAT) aggression and cuproptosis. Under RT, reactive oxygen species (ROS) are generated and consume GSH, leading to cuproptosis. The decreasing of GSH content in tumor tissues can improve the treatment effect of RT by inhibiting self-repair of tumor cells, hindering cell survival and proliferation. The combination of PC and RT alleviate tumor growth, reaching a tumor growth inhibition rate of 93.0%.
Conclusion: This tumor-specific targeting nano platform is a valuable radiosensitizer responsive to TME for improving therapeutic efficacy against tumors.
Keywords: platelet cell membrane, radiosensitization, tumor microenvironment, cuproptosis, tumor therapy

Introduction

Cancer remains a significant public health issue worldwide.[1–4] Cancer treatment strategy involves surgery, chemotherapy, radiotherapy (RT), and immunotherapy.[5,6] RT is an important multidisciplinary management of many types of cancer. It exerts high energy beams to target tumor tissue, causing oxidative stress and DNA double-strand breaks (DSBs), which in turn trigger cell apoptosis. This treatment can serve as a curative strategy for early-stage cancer, a method to control local recurrence, and palliative care for advanced cancer.[7,8] However, the tumors are much less sensitive than late-responding healthy tissues, due to tumor radioresistance resulting from specific tumor microenvironment (TME).[9,10] Thus, the use of RT should be carefully weighed to overcome radioresistance and reduce side effects. Therefore, it is urgent to develop a novel method for improving the efficacy of RT.

Radiosensitizers have been applied for the improvement of RT during clinic, such as cisplatin, antibody-drug conjugates (ADC) and epoxygenase-2 inhibitors.[11–15] But these sensitizers have serious side effects.[16–18] Recently, nanotechnology can improve RT treatment effects and overcome the above limitations.[19,20] Nanoplatforms containing high Z elements can accumulate large dosages by increasing the amounts of photoelectrons and Auger electrons. Ertas's team developed an alginate coated Pt nanoradiosensitizer for breast cancer.[21] Han et al found that Au infinite

Received: 24 November 2024
Accepted: 11 March 2025
Published: 19 March 2025

coordination complex causes dose enhancement after the metal-organic nanocomplex entry to cells.[22] Cao reported that platinum nano-assemblies can not only act as radiosensitizers enhance radiodynamic therapy and activate immunotherapy against tumors but also contrast agent for computed tomography imaging.[23] Meanwhile, the exogenous stimuli-responsive therapy strategy by merging photothermal therapy, photodynamic therapy, ultrasonic therapy and other treatments with RT showed potential in removal of tumors.[24–26] For instance, nanoagents for dual enhancement of photothermal therapy and RT lead to synergistic effects. This was due to the hypoxia in TME can be alleviated by the accelerated blood flow induced by photothermal therapy, which results in enhancement of RT.[27,28] However, it is necessary to consider the TME triggered burst release of nanoradiosensitizer to reduce toxicity to normal tissues. It is well known, the TME is characterized by high levels of glutathione (GSH), and H_2O_2 with hypoxia status under low pH.[29,30] Responsive to these endogenous stimulations, nanoplatforms are widely developed in biomedical applications to enhance radiosensitization. An acid-triggered aggregation gold nanosystem realizes controllable size monitoring by changing the surface charge after the nanosystem accumulates in tumor regions by enhanced permeability and retention (EPR) effects.[31] Janus nanoparticles were fabricated which dissolved responsive to GSH to improve RT.[32] These smart designs of stimuli-nanoplatform enhance radio sensitization efficacy. However, positive tumor-targeting properties are necessary when considering the circulation time and side effects.

Cuproptosis, which was discovered recently, has provided novel ideas for cancer treatment.[33,34] Cuproptosis is caused by DLAT aggression and Fe-S cluster protein loss, which causes proteotoxic stress and cell death. In addition, immunogenic cell death (ICD) can be triggered by cuproptosis.[35–37] However, the cuproptosis was hindered due to the lack of transporter proteins and high level of GSH content in TME which eliminate copper ions.[38] Based on this background, here this work constructed a copper-doped polydopamine nanoparticles (PDA@Cu) and camouflaged them with platelet cell membrane (PCM), as shown in Scheme 1. This PCM coating PDA@Cu was termed PC NPs. Because platelet cells tend to accumulate in the inflammatory tumor sites, PC with PCM coating is capable of highly accumulating

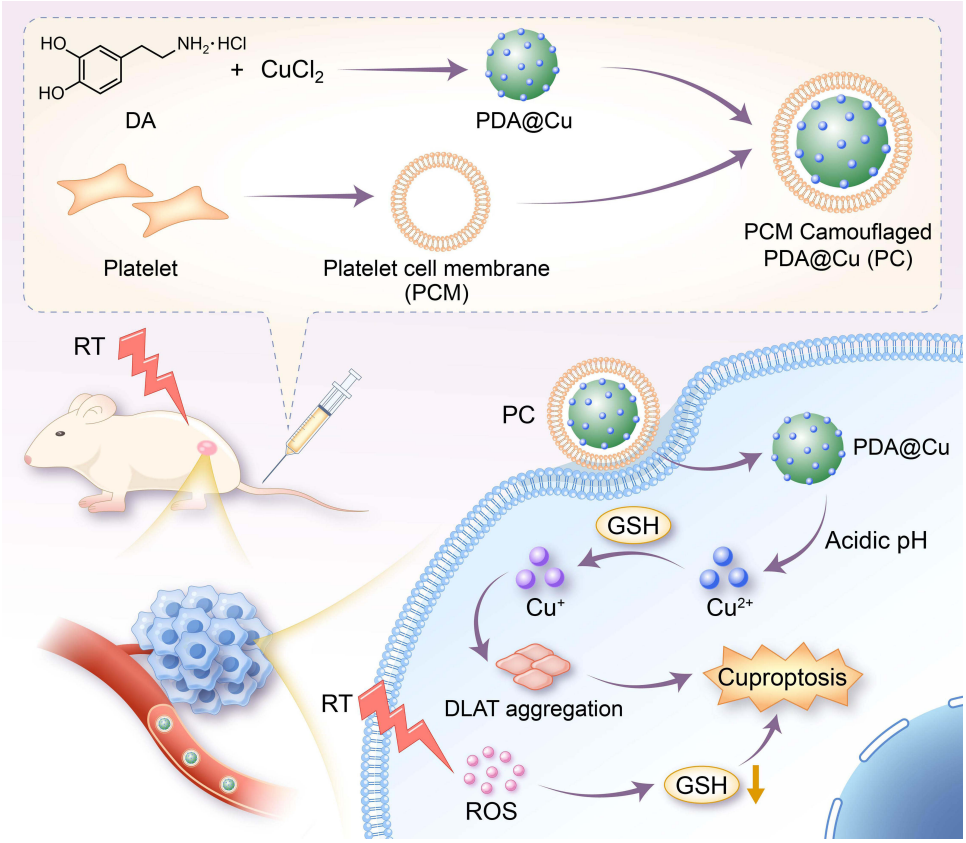

Scheme 1 Schematic illustration of synthesize procedure and functional pattern of PC NPs.

in tumor sites. Meanwhile, the disguise of PCM enables escape of PC from immune system clearance, prolonging circulation time and enhancing the delivery efficiency. After intracellular entry, PC NPs cracked and dissolved to release PDA@Cu, the latter of which dissembled under acidic TME and releases Cu^{2+}. This process enabled an influx of copper ions in tumor cells. Cu^{2+} next was reduced to more toxic Cu^{+} in the existence of GSH. Cu^{+} leads to aggregation of DLAT to further enhance the cuproptosis. RT also led to generations of reactive oxygen species (ROS) causing oxidative stress, which decreases the amount of GSH and hence strengthens the cuproptosis. Copper overloading also promoted the enhancement of RT by exhausting the intracellular GSH to inhibit tumor cell self-repair. Hereby, this cuproptosis involved PC NPs with improved tumor targeting ability, and showed potential in radiosensitization.

Result and Discussion

Characterization of Acidic pH Responsive PC NPs

PDA@Cu was prepared by using $CuCl_2$ and PDA as precursors in dispersion and stable solution (Supporting information, Experimental section). Figure 1A shows the transmission electron microscopy (TEM) images of sphere structures of PDA@Cu. After the coating of PCM, a thin film boundary appeared on the edge of PC NPs (Figure 1B). Then, the dynamic light scattering (DLS) confirmed that the average diameter of PCM NPs remained stable in both PBS and FBS over 7 days observation (Figure 1C). To further verify the characterization of PCM on PDA@Cu, the diameter and zeta potential of PDA@Cu, PC, and PCM were measured, as shown in Figure 1D. Before camouflaging of PCM whose diameter is about 188.6 nm, the diameter of PDA@Cu was increased from 123.1 nm to 139.2 nm. Meanwhile, the zeta potential of PC shifted from

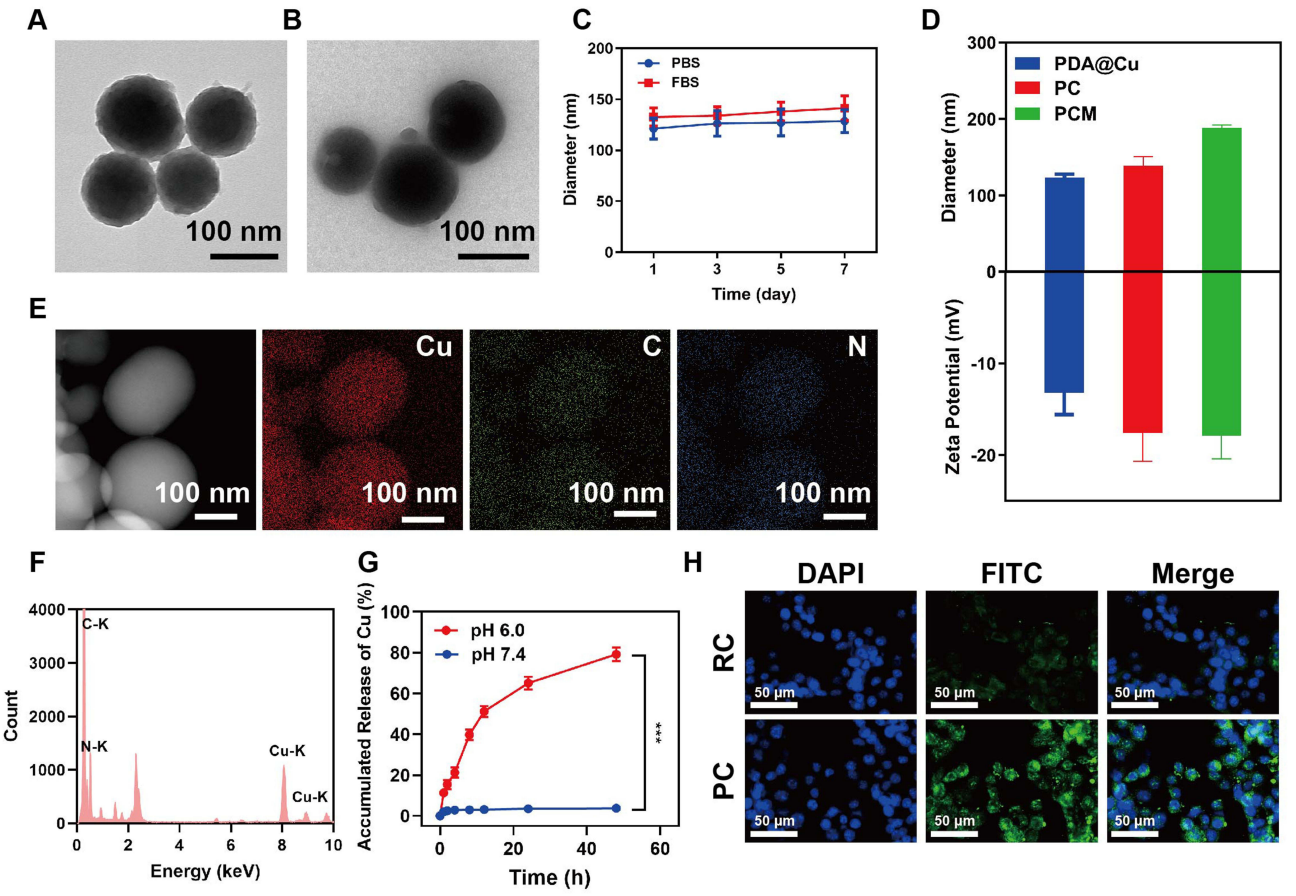

Figure 1 Characterization of PC. (**A**) TEM images of PDA@Cu NPs. (**B**) TEM images of PC NPs. (**C**) Time-dependent observation of PC diameter in PBS and FBS respectively. (**D**) Average diameter and zeta potential of PDA@Cu, PC and PCM respectively. (**E**) Elemental mapping of PC. (**F**) XPS survey of PC. (**G**) Release profile of Cu in buffer solution of different pH values. (**H**) Representative fluorescence imaging of cellular uptake in 4T1 after FITC labeled RC and PC. Data are presented as mean ± SD. *Student t* test. *** p< 0.001.

https://doi.org/10.2147/IJN.S504148

−13.2 mV (PDA@Cu) to −17.6 mV (PC) after coating of PCM (−17.9 mV). These results verified the successful coating of PCM on PC NPs. Elemental mapping patterns and Energy-dispersive X-ray spectroscopy (EDX) were used to confirm the composition of PC NPs, as shown in Figure 1E and F. The results confirmed the existence of Cu, N and C elements, and these elements were distributed in PC NPs uniformly.

The release behavior of Cu at different pH buffers was further investigated, as shown in Figure 1G. Almost no significant ion Cu release was detected in a buffer with pH 7.4. While significant amount of Cu content was observed in the buffer of the group with a pH value of 6.0, reaching as high as 79.2% amount of total Cu.

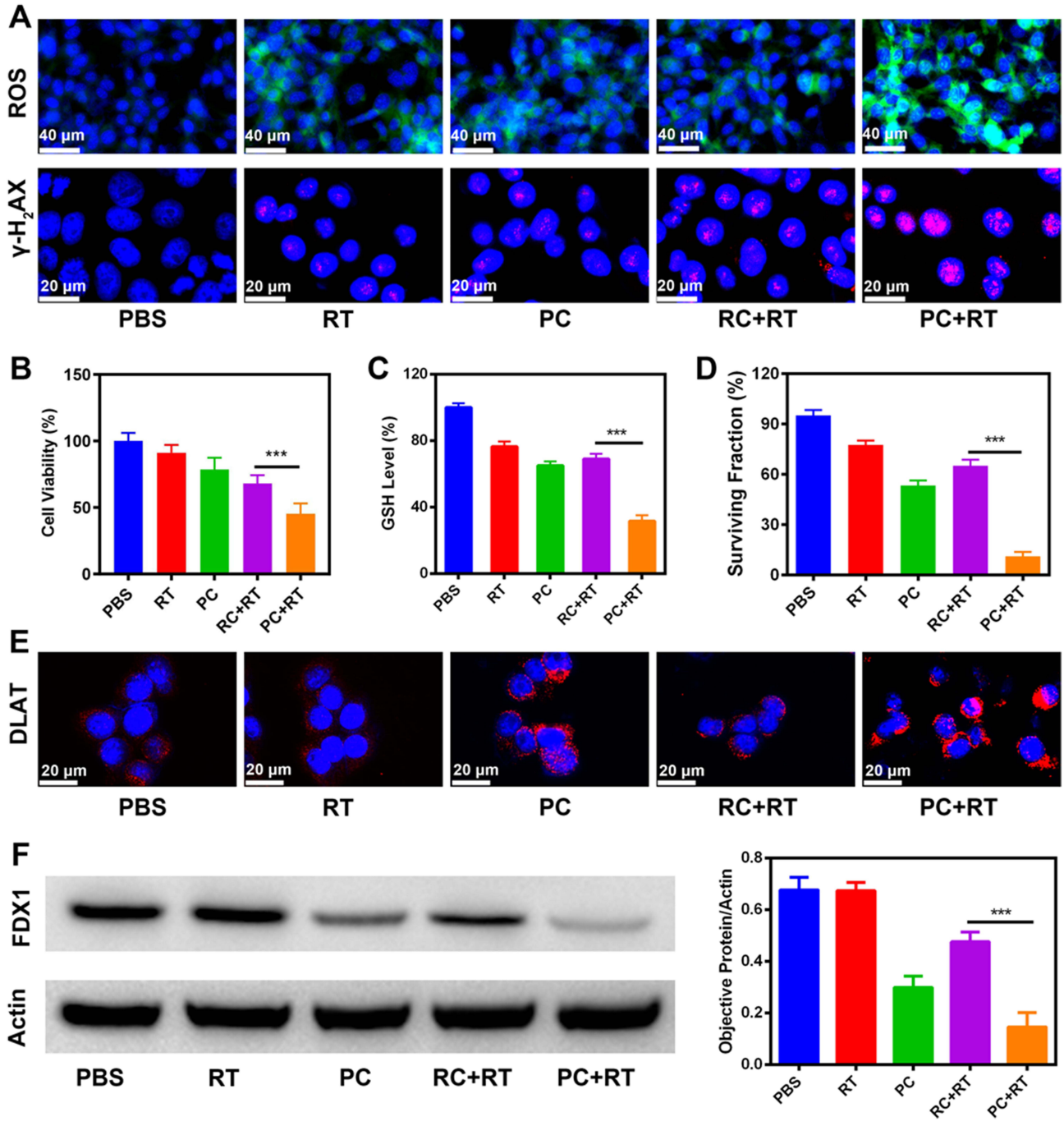

Figure 2 PC NPs could radiosensitize by inducing cuproptosis. (**A**) ROS production and DNA damage in 4T1 cells after different treatments (RT: radiotherapy). (**B**) Cell viability in all treatment groups on CT26 cells. (**C**) Measurement of GSH level. (**D**) Surviving fraction in each group. (**E**) Immunofluorescence staining of DLAT. (**F**) WB analysis and gray analysis. Data are presented as mean ± SD. *Student t* test. *** p< 0.001.

In this work, 4T1, CT26 and MCF-10A cells were obtained from purchased from the Pricella Biotechnology (China). To evaluate and compare the cellular uptake efficacy of PC NPs, erythrocyte membrane camouflaged PDA@Cu (termed RC) was also synthesized. 4T1 cells were co-incubated with either FITC-labeled RC or PC NPs, respectively. Next, the cells were fixed for measurements of the number of NPs cellular uptake by CLSM imaging. A significant amount of green fluorescence representing NPs was observed in the PC NPs treatment group (Figure 1H) than that of RC NPs group, indicating higher intracellular entry and accumulation of PC NPs.

Evaluation of Anti-Tumor Effect of PC NPs Enhanced RT

The cytotoxicity of both RC and PC NPs on MCF-10A was verified through CCK8 method based on the studies in the previous section. As shown in Figure S1, cell viability of MCF-10A decreased with RC or PC NPs concentrations increase, which exceeded 90% survival rate under 30 μg/mL Cu concentration, suggesting satisfied biocompatibility at the concentration of 30 μg/mL. The antitumor efficacy in vitro was further evaluated. As highly reactive molecules, ROS with strong oxidation property can lead to cell death. The ROS production after various treatments was assessed using DCFH-DA probe. As shown in Figure 2A, the intensity of green fluorescence was strongest in PC+RT group among all groups, while weaker intensity was observed in RC+RT group. This result indicated that significant amount of ROS was generated by PC+RT under GSH conditions at acidic buffer due to the PCM coating. Because ionization irradiation can induce cell death by direct DNA damage, γ-H_2AX staining was used for DNA DSBs staining. Slight red fluorescence was observed in 4T1 cells under RT. In addition, RC combined with RT exerted apparent DNA damage on 4T1 cells, however remarkable amount of red fluorescence intensity appeared in PC+RT group. The fluorescence intensity evaluation further confirmed the result, as shown in Figure S2. Next, cell viability evaluation was performed using CCK8 kit on CT26. As shown in Figure 2B, PC group showed modestly reduced cell viability while RC+RT group obviously destroy tumor cells. By striking contrast, PC+RT significantly killed tumor cells. Next, GSH consumption in different groups was qualified in Figure 2C. It showed that the GSH level decreased in RT group and PC group because RT exhausted GSH content and cuproptosis process of PC in cells. Compared with RC+RT group, PC+RT group showed more robust GSH elimination efficacy. The cancer cell proliferation in all groups was assessed by colony formation assay, as shown in

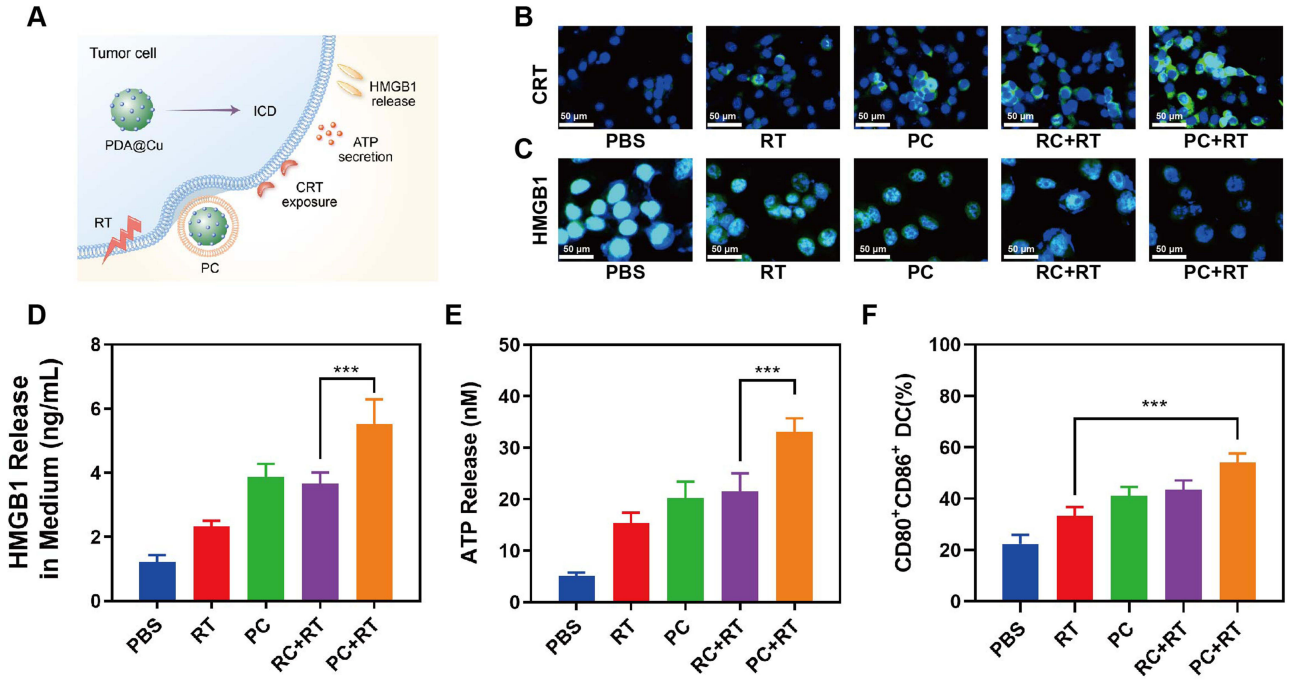

Figure 3 ICD effect assessment in vitro. CLSM for (**A**) Schematic illustration for PC+RT induced ICD (**B**)CRT efflux detection and (**C**) HMGB1 release and (**D**) HMGB1 release in medium. (**E**) Released ATP detection. (**F**) DC maturation. Data are presented as mean ± SD. *Student t* test. *** p< 0.001.

https://doi.org/10.2147/IJN.S504148

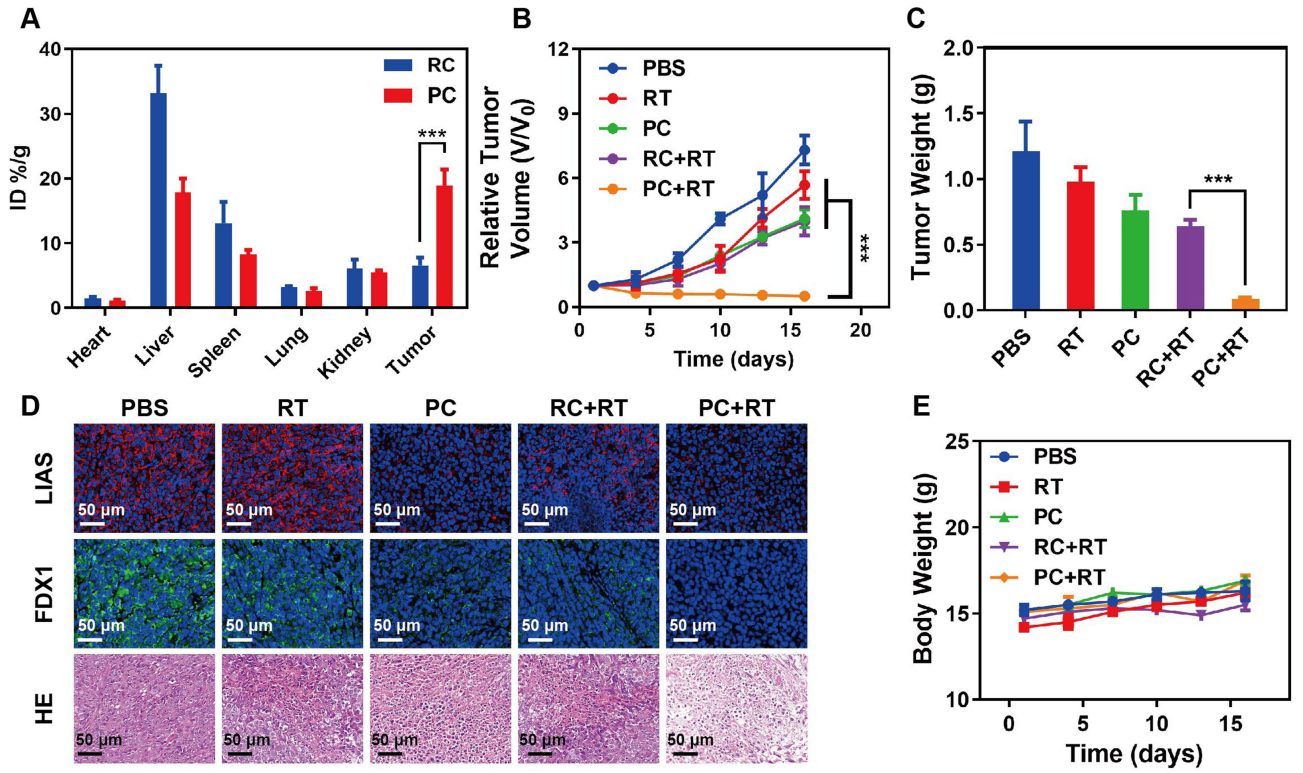

Figure 4 Identification of PC enhanced RT in tumor growth inhibition in vivo. (**A**) Biodistribution in main organs and tumors after administration of RC or PC NPs respectively. (**B**) Relative tumor volume curve. (**C**) Immunofluorescence staining of LIAS and FDX1, HE staining. (**D**) Tumor weight measurement. (**E**) Body weight fluctuation. Data are presented as mean ± SD. *Student t* test. *** p< 0.001.

Figure 2D. The surviving fraction of 4T1 cancer cells and CT26 cancer cells reduced to 10% in PC+RT group. It shows that this therapy is effective for breast cancer and colon cancer.

Subsequently, the cuproptosis induced by PC+RT was assessed. As an important intracellular signaling related to cuproptosis, DLAT aggression was investigated by fluorescence staining (Figure 2E). A large amount of DLAT was observed in 4T1 cells treated with PC NP, indicating that PC can induce cuproptosis. PC+RT showed the most significant DLAT aggression. Ferredoxin 1 (FDX1) showed an important role in copper metabolism, since it involved in the Fe-S proteins and electron transfer processes.[37] From the result of Western blot analysis and protein quantification, the FDX1 downregulated after the PC treatment (Figure 2F). This confirmed that the cuproptosis was induced by PC. Surprisingly, PC combined RT exhibited the most obvious downregulation of FDX1 protein. These above results verified that both RT and PC can consume intracellular GSH, PC showed higher cellular uptake of RC which increased the antitumor efficacy in vitro. The PC showed potential in inducing cuproptosis, while the cuproptosis was more robust in combination therapy of PC and RT.

Promotion of ICD by PC NPs Enhanced RT via Cuproptosis

ICD can activate immune response, which is characterized by damage-associated molecular patterns (DAMPs) including releasing of ATP, surface-exposed calreticulin (CRT) and DNA bound high-mobility histone 1 (HMGB1). An experiment in vitro was designed for the study of in vitro ICD induction and dendritic cell (DC) maturation assays of 4T1 cells (Figure 3A). The ICD-related DAMPs by fluorescence imaging under various treatment groups were tested. The "eat me" signal of CRT was observed using CLSM imaging (Figure 3B). Negligible amounts of green fluorescence were observed in RT or PC or RC+RT treatment groups. However, PC+RT treatment group exhibited significant amount of CRT exposure among all groups. Besides, significant amount of HMGB1 was released into medium after treatment of PC+RT group (Figure 3C and D), which was 1.50 times higher than that of RC+RT group. Meanwhile, PC+RT group had the highest relative concentration of ATP, which was 1.54 times higher than that of RC+RT group (Figure 3E). Maturated

mouse bone marrow-derived DCs were incubated with pretreated 4T1 cells before using flow cytometry to assess the DC maturation, as shown in Figure 3F. PC+RT showed the highest population of mature DC proportion, reaching as high as 54.1% $CD80^{+}CD86^{+}$ DC, which was significantly higher than that of RT group. These results indicated a more robust ICD effect after the addition of PC, suggesting the radiosensitization by PC.

Antitumor Efficacy Evaluation on Subcutaneous Tumor Model

Tumor-specific targeting in vivo was studied on subcutaneous 4T1 tumor bearing mice. Animal experiments were conducted following the guidelines of the National Institutes of Health and approved by the Animal Ethics Committee of Guangxi Medical University (Approval number: 2023-KY (0932)). 10^5 4T1 cells were subcutaneously injected on the

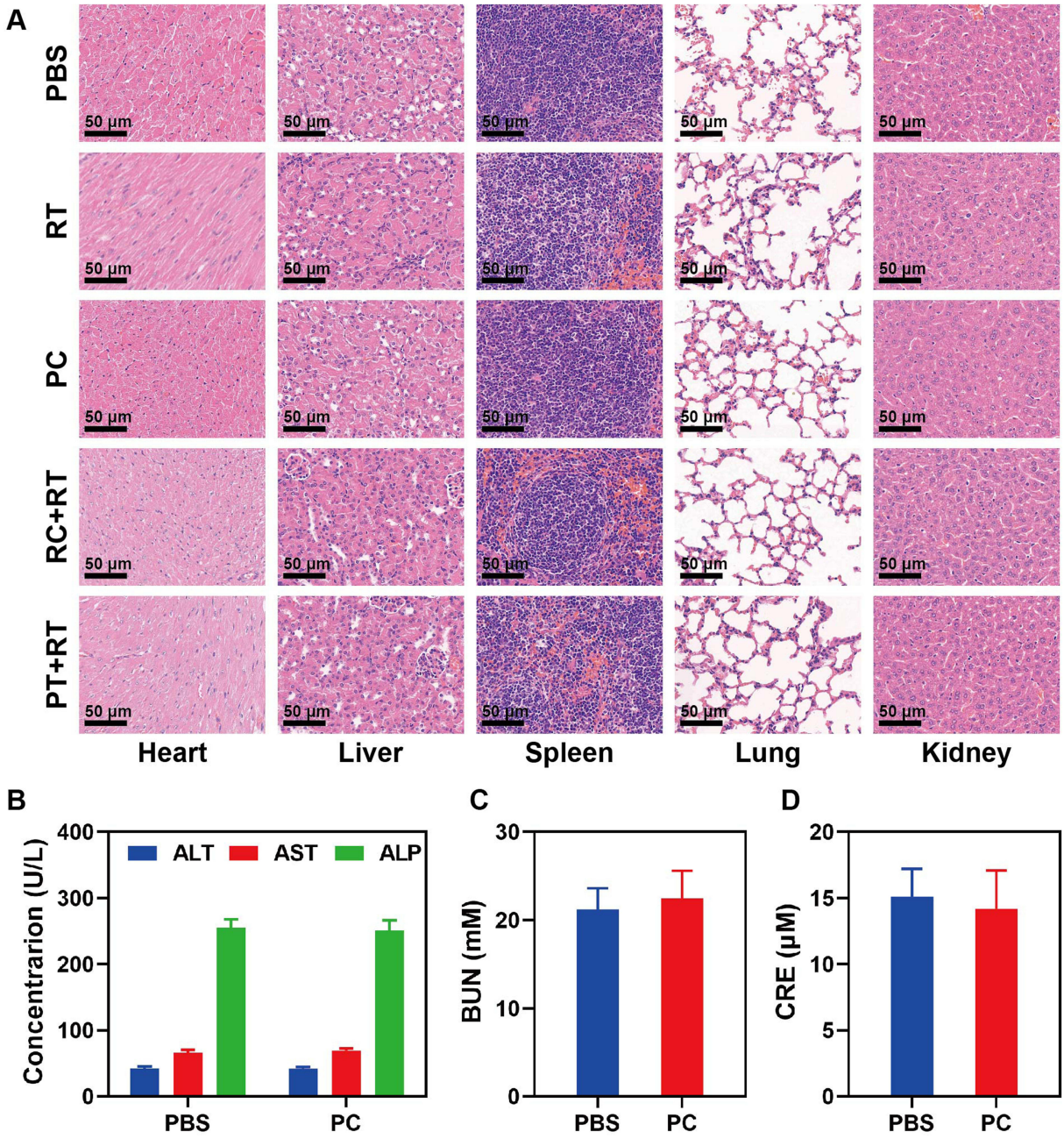

Figure 5 Observation of biosafety. (**A**) Identification of damage to main organs with HE staining analysis. (**B**) The ALT, AST and ALP levels in mice received injection of PBS and PC. (**C**) BUN and (**D**) CRE concentration in PBS and PC treatment groups.

https://doi.org/10.2147/IJN.S504148

right lap of 6-week-old female BALB/c mice to form tumor models. After 24 h injection of RC or PC NPs via tail vein, Cu concentration biodistribution in main organs and tumors was quantified using ICP-AES, as shown in Figure 4A. The results confirmed that PC had higher tissue accumulation than that of RC, implying PC NPs had significant active tumor targeting ability than RC. Besides, the subcutaneous 4T1 tumor bearing model on BALB/c mice was established to examine the antitumor efficacy of this integral method. The day 1 was set as the next day of treatment and all the mice were executed at day 16, as shown in Figure 4B. Mild tumor inhibition was observed under treatment of RT alone, while obvious tumor suppressing was observed in RC+RT group. Surprisingly, integral treatment of PC+RT was proven to be the most efficient strategy among all, significantly higher than that of other groups, which was consistent with the results in Figure 4C.

Immunofluorescence and HE staining were further performed. Lipoic acid synthetase (LIAS) and FDX1 play important roles in influencing cuproptosis. The tumor tissue of PC+RT treatment exhibited decreasing expression of LIAS with minimal red fluorescence intensity, as confirmed in Figure 4D. PC+RT treatment also effectively promoted FDX1 reduction. And most substantial cell death was observed in PC+RT group. These in vivo results demonstrated that the integral treatment of PC and RT showed potential in tumor growth inhibition.

Moreover, body weight had no significant change after these treatment strategies (Figure 4E). It is necessary to evaluate the biosafety of nano-radiosensitizers for cancer treatment. Therefore, the biosafety of PC NPs in vivo was then further evaluated. Ten healthy mice received administration of PBS buffer or PC NPs solution and were executed after 10 days. Histological analysis of main organs including heart, liver, spleen, lung and kidney confirmed positive compatibility of PC NPs, as shown in Figure 5A. In addition, blood biochemical analyses of alanine transaminase (ALT), aspartate transaminase (AST), alkaline phosphatase (ALP), blood urea nitrogen (BUN) and creatinine (CRE) were evaluated, and found that there was no significant difference between PBS and PC group (Figure 5B–D).

Conclusion

This work developed a biomimicking TME responsive cuproptosis induced nanoplatform PC for radiosensitization. PC NPs can efficiently target and accumulate tumor tissues through PCM camouflage. Since the high cellular uptake property of PC NPs, PDA@Cu is successful transport into cells. Under acidic TME, PDA@Cu is dissembled in cell matrix, releasing a burst of Cu^{2+} ions which consume reducible GSH to generate Cu^{+}. Next, Cu^{+} induces DLAT aggression occurred under RT irradiation. Meanwhile, ROS generated from RT also lead to decreasing GSH content. Both Cu^{+} and RT lead to severe cell cuproptosis, enhance ICD effect in vitro, and promote DC maturation. The antitumor efficacy of integral treatment of PC and RT is significant as proven both in vitro and in vivo. This work hereby provided a potential strategy by radiosensitization induced by PC to enhance cuproptosis, holding great promise in the treatment of cancer.

Acknowledgments

We previously published an article on cuproptosis (reference [37]). The published article used Cu doped polypyrrole nanoparticles loaded with BPTES, which can release copper ions upon hydrogen peroxide stimulation and exhibit POD like enzyme activity. Combined with BPTES mediated glutamine metabolism, it enhances cuproptosis treatment. The innovation of this work is reflected in the BPTES sensitization of cuproptosis mediated by nanoparticles.

In this work, we used polydopamine nanoparticles that adsorb copper ions, which are significantly different from previously published nanomedicine. These nanoparticles release copper ions under acidic conditions, causing cuproptosis in tumor cells and enhancing the sensitivity of radiation immunotherapy. This work focuses on the application of cuproptosis in RT immune-sensitization, and there is currently limited research on this topic.

Funding

We are grateful for the financial support from the Shenzhen Science and Technology Program (JCYJ20220530153816038).

Disclosure

The authors report no conflicts of interest in this work.

References

1. Taylor C, Dodwell D, McGale P, et al. Radiotherapy to regional nodes in early breast cancer: an individual patient data meta-analysis of 14324 women in 16 trials. *Lancet*. 2023;402(10416):1991–2003. doi:10.1016/S0140-6736(23)01082-6
2. Jagsi R, Griffith KA, Harris EE, et al. Omission of Radiotherapy After Breast-Conserving Surgery for Women With Breast Cancer With Low Clinical and Genomic Risk: 5-Year Outcomes of IDEA. *J Clin Oncol*. 2023;42(4):390–398. doi:10.1200/JCO.23.02270
3. Siegel RL, Miller KD, Wagle NS, Jemal A. Cancer statistics, 2023. *Ca a Cancer J Clin*. 2023;73(1):17–48. doi:10.3322/caac.21763
4. Siegel RL, Giaquinto AN, Jemal A. Cancer statistics, 2024. *Ca a Cancer J Clin*. 2024;74(1):12–49. doi:10.3322/caac.21820
5. Ashrafizadeh M, Zarrabi A, Bigham A, et al. (Nano)platforms in breast cancer therapy: drug/gene delivery, advanced nanocarriers and immunotherapy. *Med Res Rev*. 2023;43(6):2115–2176. doi:10.1002/med.21971
6. Gautam S, Marwaha D, Singh N, et al. Self-Assembled Redox-Sensitive Polymeric Nanostructures Facilitate the Intracellular Delivery of Paclitaxel for Improved Breast Cancer Therapy. *Mol Pharmaceut*. 2023;20(4):1914–1932. doi:10.1021/acs.molpharmaceut.2c00673
7. Haussmann J, Corradini S, Nestle-Kraemling C, et al. Recent advances in radiotherapy of breast cancer. *Radiat Oncol*. 2020;15(1):71. doi:10.1186/s13014-020-01501-x
8. Liu L, Yang Y, Guo Q, et al. Comparing hypofractionated to conventional fractionated radiotherapy in postmastectomy breast cancer: a meta-analysis and systematic review. *Radiat Oncol*. 2020;15(1):17. doi:10.1186/s13014-020-1463-1
9. Wang J, Han Y, Li Y, et al. Targeting Tumor Physical Microenvironment for Improved Radiotherapy. *Small Methods*. 2022;6(11):2200570. doi:10.1002/smtd.202200570
10. Wu Y, Song Y, Wang R, Wang T. Molecular mechanisms of tumor resistance to radiotherapy. *mol Cancer*. 2023;22(1):96. doi:10.1186/s12943-023-01801-2
11. Schuette A, Lander DP, Kallogjeri D, et al. Predicting Hearing Loss After Radiotherapy and Cisplatin Chemotherapy in Patients With Head and Neck Cancer. *JAMA Otolaryngol Head Neck Surg*. 2020;146(2):106–112. doi:10.1001/jamaoto.2019.3550
12. Provencio M, Majem M, Guirado M, et al. Phase II clinical trial with metronomic oral vinorelbine and tri-weekly cisplatin as induction therapy, subsequently concomitant with radiotherapy (RT) in patients with locally advanced, unresectable, non-small cell lung cancer (NSCLC). Analysis of survival and value of ctDNA for patient selection. *Lung Cancer*. 2021;153:25–34. doi:10.1016/j.lungcan.2021.01.005
13. Lebow ES, Pike LRG, Seidman AD, Moss N, Beal K, Yu Y. Symptomatic Necrosis With Antibody-Drug Conjugates and Concurrent Stereotactic Radiotherapy for Brain Metastases. *JAMA Oncol*. 2023;9(12):1729–1733. doi:10.1001/jamaoncol.2023.4492
14. Zhao M, Zhao L, Yang H, Duan Y, Li G. Apparent diffusion coefficient for the prediction of tumor response to neoadjuvant chemo-radiotherapy in locally advanced rectal cancer. *Radiat Oncol*. 2021;16(1):17. doi:10.1186/s13014-020-01738-6
15. Zhang S, Jiang Y, Shi L, et al. Identification and analysis of key genes related to efferocytosis in colorectal cancer. *BMC Med Genomics*. 2024;17(1):198. doi:10.1186/s12920-024-01967-8
16. Barazzuol L, Coppes RP, van Luijk P. Prevention and treatment of radiotherapy-induced side effects. *Mol Ooncol*. 2020;14(7):1538–1554. doi:10.1002/1878-0261.12750
17. Zheng N, Wang Q, Li C, et al. Responsive Degradable Theranostic Agents Enable Controlled Selenium Delivery to Enhance Photothermal Radiotherapy and Reduce Side Effects. *Adv Healthcare Mater*. 2021;10(10):2002024. doi:10.1002/adhm.202002024
18. Piraux E, Caty G, Aboubakar Nana F, Reychler G. Effects of exercise therapy in cancer patients undergoing radiotherapy treatment: a narrative review. *SAGE Open Med*. 2020;8:2050312120922657. doi:10.1177/2050312120922657
19. Nosrati H, Salehiabar M, Charmi J, et al. Enhanced In Vivo Radiotherapy of Breast Cancer Using Gadolinium Oxide and Gold Hybrid Nanoparticles. *ACS Appl Bio Mater*. 2023;6(2):784–792. doi:10.1021/acsabm.2c00965
20. Colak B, Ertas YN. Implantable, 3D-Printed Alginate Scaffolds with Bismuth Sulfide Nanoparticles for the Treatment of Local Breast Cancer via Enhanced Radiotherapy. *ACS Appl Mater Interfaces*. 2024;16(13):15718–15729. doi:10.1021/acsami.3c17024
21. Rashidzadeh H, Seidi F, Ghaffarlou M, et al. Preparation of alginate coated Pt nanoparticle for radiosensitization of breast cancer tumor. *Int J Biol Macromol*. 2023;233:123273. doi:10.1016/j.ijbiomac.2023.123273
22. Wang J, Zhao J, Ma F, et al. One Stone, Two Birds: a Peptide-Au(I) Infinite Coordination Supermolecule for the Confederate Physical and Biological Radiosensitization in Cancer Radiation Therapy. *Small*. 2023;19(11):2204238. doi:10.1002/smll.202204238
23. Zhang F, Feng L, Jia C, et al. Mixed-valence Pt(0)/Pt^{2+} nanoassemblies as high-Z radiosensitizers and metallo-immune regulators for potent radiotherapy of breast cancer. *Nano Today*. 2023;48:101708. doi:10.1016/j.nantod.2022.101708
24. Zhang Y, Liu J, Yu Y, et al. Enhanced radiotherapy using photothermal therapy based on dual-sensitizer of gold nanoparticles with acid-induced aggregation. *Nanomedicine*. 2020;29:102241. doi:10.1016/j.nano.2020.102241
25. Sun Q, Wu J, Jin L, et al. Cancer cell membrane-coated gold nanorods for photothermal therapy and radiotherapy on oral squamous cancer. *J Mater Chem B*. 2020;8(32):7253–7263. doi:10.1039/D0TB01063D
26. Lyu M, Luo M, Li J, et al. Personalized Carbon Monoxide-Loaded Biomimetic Single-Atom Nanozyme for Ferroptosis-Enhanced FLASH Radioimmunotherapy. *Adv Funct Mater*. 2023;33(51):2306930. doi:10.1002/adfm.202306930
27. Luo M, Zhu X, Yang H, et al. Fabrication of AuPt heterostructured nanorings for enhanced synergistic radio-photothermal therapy. *Nano Today*. 2023;51:101919. doi:10.1016/j.nantod.2023.101919
28. Peltek OO, Karpov TE, Rogova A, et al. Development of Nanocarrier-Based Radionuclide and Photothermal Therapy in Combination with Chemotherapy in Melanoma Cancer Treatment. *ACS Appl Mater Interfaces*. 2023;15(10):13460–13471. doi:10.1021/acsami.2c20619
29. Arneth B. Tumor Microenvironment. *Medicina*. 2019;56(1):15. doi:10.3390/medicina56010015
30. Whiteside TL. The tumor microenvironment and its role in promoting tumor growth. *Oncogene*. 2008;27(45):5904–5912. doi:10.1038/onc.2008.271
31. Zhang Y, Huang F, Ren C, et al. Enhanced Radiosensitization by Gold Nanoparticles with Acid-Triggered Aggregation in Cancer Radiotherapy. *Adv Sci*. 2019;6(8):1801806. doi:10.1002/advs.201801806
32. Lin X, Zhu R, Hong Z, et al. GSH-Responsive Radiosensitizers with Deep Penetration Ability for Multimodal Imaging-Guided Synergistic Radio-Chemodynamic Cancer Therapy. *Adv Funct Mater*. 2021;31(24):2101278. doi:10.1002/adfm.202101278
33. Tang D, Chen X, Kroemer G. Cuproptosis: a copper-triggered modality of mitochondrial cell death. *Cell Res*. 2022;32(5):417–418. doi:10.1038/s41422-022-00653-7

34. Chen L, Min J, Wang F. Copper homeostasis and cuproptosis in health and disease. *Signal Transduction and Targeted Therapy*. 2022;7(1):378. doi:10.1038/s41392-022-01229-y
35. Zhao P, Wang H, Zhao H, et al. Tumor microenvironment-reprogrammable CpG-templated copper sulfide loaded with disulfiram for sensitized cuproptosis immunotherapy. *Chem Eng J*. 2024;487:150524. doi:10.1016/j.cej.2024.150524
36. Huang Q, Liang J, Chen Q, et al. Metal-organic framework nanoagent induces cuproptosis for effective immunotherapy of malignant glioblastoma. *Nano Today*. 2023;51:101911. doi:10.1016/j.nantod.2023.101911
37. Zhang N, Ping W, Rao K, et al. Biomimetic copper-doped polypyrrole nanoparticles induce glutamine metabolism inhibition to enhance breast cancer cuproptosis and immunotherapy. *J Control Release*. 2024;371:204–215. doi:10.1016/j.jconrel.2024.05.045
38. Xie J, Yang Y, Gao Y, He J. Cuproptosis: mechanisms and links with cancers. *mol Cancer*. 2023;22(1):46. doi:10.1186/s12943-023-01732-y